Simulations of toroidal Alfvén eigenmode excited by fast ions on the Experimental Advanced Superconducting Tokamak

Simulations of toroidal Alfvén eigenmode excited by fast ions on the Experimental Advanced Superconducting Tokamak

Cite as: Phys. Plasmas **25**, 052503 (2018); https://doi.org/10.1063/1.5023538
Submitted: 25 January 2018 • Accepted: 23 April 2018 • Published Online: 09 May 2018

Youbin Pei, Nong Xiang, Wei Shen, et al.

Simulations of toroidal Alfvén eigenmode excited by fast ions on the Experimental Advanced Superconducting Tokamak

Youbin Pei,[1,2,3] Nong Xiang,[1,a)] Wei Shen,[1,b)] Youjun Hu,[1] Y. Todo,[4] Deng Zhou,[1] and Juan Huang[1]
[1]*Institute of Plasma Physics, Chinese Academy of Sciences, Hefei, Anhui 230031, China*
[2]*University of Science and Technology of China, Hefei, Anhui 230026, China*
[3]*Center for Magnetic Fusion Theory, Chinese Academy of Sciences, Hefei, Anhui 230031, China*
[4]*National Institute for Fusion Science, Toki, Gifu 509-5292, Japan*

(Received 25 January 2018; accepted 23 April 2018; published online 9 May 2018)

Kinetic-MagnetoHydroDynamic (MHD) hybrid simulations are carried out to study fast ion driven toroidal Alfvén eigenmodes (TAEs) on the Experimental Advanced Superconducting Tokamak (EAST). The first part of this article presents the linear benchmark between two kinetic-MHD codes, namely MEGA and M3D-K, based on a realistic EAST equilibrium. Parameter scans show that the frequency and the growth rate of the TAE given by the two codes agree with each other. The second part of this article discusses the resonance interaction between the TAE and fast ions simulated by the MEGA code. The results show that the TAE exchanges energy with the co-current passing particles with the parallel velocity $|v_\parallel| \approx V_{A0}/3$ or $|v_\parallel| \approx V_{A0}/5$, where V_{A0} is the Alfvén speed on the magnetic axis. The TAE destabilized by the counter-current passing ions is also analyzed and found to have a much smaller growth rate than the co-current ions driven TAE. One of the reasons for this is found to be that the overlapping region of the TAE spatial location and the counter-current ion orbits is narrow, and thus the wave-particle energy exchange is not efficient. *Published by AIP Publishing*. https://doi.org/10.1063/1.5023538

I. INTRODUCTION

Fast ions in tokamaks produced by fusion reactions, neutral beam injection (NBI) and RF heating can excite toroidal Alfvén eigenmodes (TAEs),[1–8] which can, in turn, enhance the transport of fast ions.[9–16] TAEs have been widely observed in experiments[17–20] and a great deal of numerical simulations have been performed to understand the interaction between TAEs and fast ions.[21–26] Several numerical models based on different physical models have been established: the gyro-fluid model,[27] the gyro-/drift-kinetic MagnetoHydroDynamic (MHD) hybrid model[28–31] and the fully gyrokinetic model.[32–35] In the kinetic-MHD hybrid model, the main plasmas are described by the MHD model and the fast ions by the gyro-/drift-kinetic model. The MEGA[36–38] and M3D-K[39] codes are two of the many codes based on the kinetic-MHD hybrid model. Both the MEGA code[13,40,41] and the M3D-K code[42–45] have been widely used to investigate Alfvén eigenmodes (AEs) and energetic particle modes (EPMs) in many tokamaks. Recently, both of the codes are used to investigate AEs and EPMs in the Experimental Advanced Superconducting Tokamak (EAST). Therefore, benchmark studies between the two codes based on realistic EAST equilibria are desired. The first part of this article presents the linear benchmark between these two codes using a realistic equilibrium from the EAST discharge #38300 at 3900 ms.[46] The fast ions generated by the deuterium NBI on the EAST are described by an anisotropic slowing down distribution in both the codes. In the typical parameter regime of EAST fast ions, the mode excited is found to be a TAE with $|n| = 1$ and $m = 1, 2$, where m and n are the poloidal and toroidal mode numbers, respectively. The two-dimensional mode structures on the poloidal plane calculated by the MEGA code and the M3D-K code are in agreement with each other. Parameter scans show that the frequency and the growth rate of the TAE given by the two codes agree with each other. The parameter scans of the TAE growth rate over the birth velocity and the central pitch angle of the fast ions show a peak near a particular value. To better explain this, the second part of this article discusses the resonance condition between the TAE and fast ions. The results show that the TAE exchanges energy with the co-current passing particles with the parallel velocity $|v_\parallel| \approx V_{A0}/3$ or $|v_\parallel| \approx V_{A0}/5$, where V_{A0} is the Alfvén speed on the magnetic axis. The resonant particles with $|v_\parallel| \approx V_{A0}/3$ are dominant. To further verify the role of $|v_\parallel| \approx V_{A0}/3$ co-current passing particles in exciting the TAE, we compare the TAE excited by fast ions with different birth velocities and injection angles, but with approximately the same parallel velocity $|v_\parallel| \approx V_{A0}/3$. The results indicate that the growth rate of the excited TAE remains the same, which shows the dominant role of the $|v_\parallel| \approx V_{A0}/3$ resonant particles. This also explains why there is a peak in the dependence of the growth rate on the fast ions' birth velocity and central pitch angle. The TAE destabilized by the counter-current passing ions is also analyzed and found to have a much smaller growth rate than the co-current ion driven TAE. One of the reasons for this is found to be that the overlapping region of the spatial location of the TAE and the counter-current ion orbits is narrow, and thus the wave-particle energy exchange is not efficient.

a)E-mail: xiangn@ipp.cas.cn
b)E-mail: shenwei@ipp.cas.cn

The remainder of this article is organized as follows: Sec. II briefly reviews the physical models of MEGA and M3D-K codes. The thermal plasma parameters used in this work are described in Sec. III. The fast ion distribution function is described in Sec. IV. The comparison of the results given by the two codes is presented in Sec. V. Section VI discusses the resonance interaction between the TAE and fast ions simulated by the MEGA code. Section VII is a brief summary.

II. PHYSICAL MODELS

Both the MEGA code[36–38] and the M3D-K code[39] describe the thermal plasma as a single fluid by using the nonlinear full MHD equations. The energetic particles (EPs) are described by drift-kinetic or gyrokinetic equations. For the $|n| = 1$ and $m = 1$, 2 TAE investigated in this paper, the perpendicular wave vector $k_\perp \approx m/a$, where a is the minor radius ($a = 0.44m$). The estimated value of $k_\perp \rho_h$ is $k_\perp \rho_h \approx \frac{m}{a} \cdot \frac{m_D v_{\text{birth}}}{eB_0} = 2.27 \times 0.035 = 0.079 \ll 1$ (ρ_h, m_D, and v_{birth} are the gyro-radius, the mass and the birth velocity of EPs, respectively, e is the elemental charge and B_0 is the magnetic field strength on the magnetic axis). This value is much smaller than 1, which roughly justifies using the drift-kinetic model.[47] In the MEGA code, the EP effects are included in the MHD momentum equation via the EP current (usually called the current coupling scheme[30]). In the M3D-K code, the EP effects are included in the momentum equation via the EP pressure (called the pressure coupling scheme[30]). The evolution of the distribution of EPs is simulated by the δf particle-in-cell method.[48,49]

III. THERMAL PLASMA PARAMETERS

The equilibrium used in MEGA is reconstructed by the EFIT code[50] based on the experimental diagnostic data for the EAST discharge #38300 at 3900 ms. The flux surface configuration and the simulation box used by MEGA are plotted in Fig. 1(a). The profiles of the electron number density n_e, the plasma pressure P, and the safety factor q are plotted in Fig. 1(b). The equilibrium used by the M3D-K code is generated from the VMEC code[51] by using the pressure and safety factor profiles reconstructed by EFIT. The equilibrium generated by VMEC is up-down symmetric.

IV. FAST ION DISTRIBUTION

The fast ions in both the codes are described by the following anisotropic slowing down distribution:

$$f_{\text{eq}}\left(\bar{\psi}_p, v, \Lambda, \sigma\right) = C \exp\left(-\frac{\bar{\psi}_p}{\psi_{\text{scale}}}\right) \frac{1}{v^3 + v_{\text{crit}}^3} \times \frac{1}{2}\text{erfc}\left(\frac{v - v_{\text{birth}}}{\Delta v}\right) \exp\left(-\frac{(\Lambda - \Lambda_0)^2}{(\Delta\Lambda)^2}\right) \cdot H(-\sigma), \quad (1)$$

where C is a constant determining the stored energy of fast ions; $\bar{\psi}_p$ is the normalized poloidal magnetic flux; ψ_{scale} is a quantity characterizing the radial gradient of fast ions; v is the velocity of fast ions; v_{crit} is the critical velocity of the collisional friction of fast ions with thermal electrons and ions being equal;[19] v_{birth} is the neutral beam injection velocity; Δv is a small velocity (compared with v_{birth}), which is used to set the cutoff width near v_{birth}; $\Lambda = \mu B_0/\varepsilon$ is the normalized magnetic moment with μ and ε being the magnetic moment and the kinetic energy of fast ions; Λ_0 and $\Delta\Lambda$ characterize the peak location and the width of the distribution over the pitch angle, respectively; $H(\sigma)$ is the Heaviside step function ($H(\sigma) = 0$ for $\sigma < 0$ and $H(\sigma) = 1$ for $\sigma > 0$); and $v_\parallel = \boldsymbol{v} \cdot \boldsymbol{b}$ is the parallel velocity of fast ions, where, $\boldsymbol{b} = \boldsymbol{B}/|\boldsymbol{B}|$ with $\boldsymbol{B}$ being the magnetic field, $\sigma = \text{sign}(v_\parallel)$ with $\sigma = -1$ and $+1$ corresponding to the co-current and the counter-current injection, respectively (the toroidal magnetic field and the plasma current are in the opposite direction of the equilibrium used in this work).

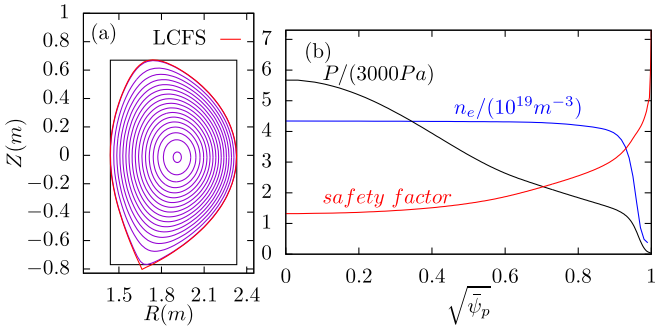

FIG. 1. (a) Magnetic surface shape of EAST discharge 38 300 at 3900 ms. The Last-Closed-Flux-Surface (LCFS) is indicated. The simulation box used in the MEGA code on the poloidal plane is also indicated, which is a rectangle with $R_{\min} < R < R_{\max}$ and $Z_{\min} < Z < Z_{\max}$, where $R_{\min}$, $R_{\max}$, $Z_{\min}$, and $Z_{\max}$ are the extreme points on the flux surface with $\sqrt{\bar{\psi}_p} = 99\%$, where $\bar{\psi}_p$ is the normalized poloidal magnetic flux. (b) Radial profiles of the thermal plasma pressure, the safety factor, and the electron number density. The safety factor and the electron number density at the magnetic axis are $q_0 = 1.32$ and $n_{e0} = 4.2 \times 10^{19}\text{m}^{-3}$, respectively. The toroidal magnetic field at the magnetic axis is $B_{\phi 0} = +1.64$ T. The toroidal plasma current is $I_{p\phi} = -398$ kA. Here, (R, ϕ, Z) is the right-handed cylindrical coordinates with R being the major radius, ϕ being the usual toroidal angel, and Z being the vertical coordinate.

In this work, we fix the following parameters in both the codes: $\psi_{\text{scale}} = 0.3$; $v_{\text{crit}} = 0.62V_{A0}$, which corresponds to the critical velocity with the electron temperature $T_e = 2$ keV, $V_{A0} = 3.837 \times 10^6$ m/s is the Alfvén velocity on magnetic axis; the cutoff width near the beam velocity is chosen as $\Delta v = 0.15V_{A0}$. Except for the parameter scanning sections, typical EAST NBI fast ion parameters are used: the injected beam velocity is chosen as $v_{\text{birth}} = 0.72V_{A0}$, corresponding to a deuteron with a kinetic energy of 80 keV, which is the maximum energy of a deuteron generated from the NBI on the EAST; the central pitch angle variable Λ_0 is chosen as $\Lambda_0 = 0.68$; the expansion width of the distribution over Λ is chosen as $\Delta\Lambda = 0.1$; and the on-axis beta value of fast ions is chosen as $\beta_{h0} = 0.5\%$.

In both MEGA and M3D-K simulations, the electrical resistivity η and the viscosity ν are chosen as $\eta = 0$ and $\nu = 10^{-5} a V_{A0} = 16.89\,\text{m}^2/\text{s}$, respectively.

The number of grid points used in the MEGA code is $(128 \times 16 \times 128)$ for cylindrical coordinates (R, ϕ, Z) and 5.2×10^5 markers are used in the linear parameter scans,

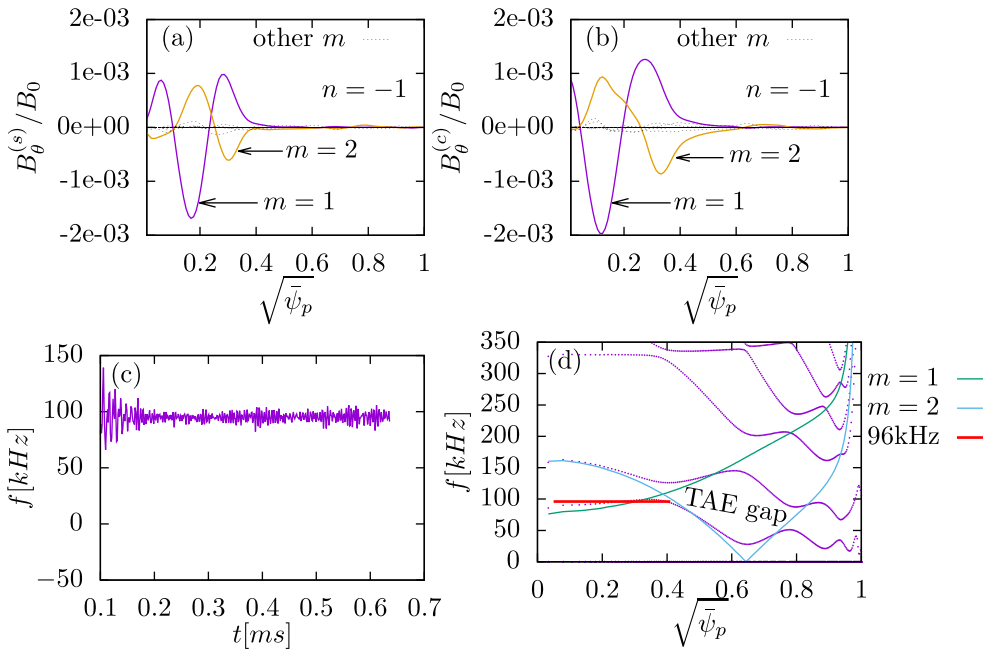

FIG. 2. Radial profiles of the sine (a) and cosine (b) parts of various poloidal harmonics of the $n=-1$ component of the perturbed poloidal magnetic field B_θ in the linear stage. (c) Time evolution of the frequency of $m/n=1/-1$ harmonic of B_θ. (d) The frequency (96 kHz) and the radial width of the TAE plotted on the $n=-1$ Alfvén continua. The $m=1$ and $m=2$ Alfven continua in the cylindrical limit are also plotted. The continua are computed by using an ideal MHD eigenvalue code GTAW.[53]

while 4×10^6 markers are used in analyzing the resonance condition between the TAE and fast ions to reduce the numerical noise. The convergence over the marker number used in the simulation has been verified. The number of grid points used in M3D-K is $(101\times12\times101)$ for cylindrical coordinates (R,ϕ,Z), and 4×10^6 particles are used in the simulations.

V. BENCHMARK BETWEEN THE MEGA CODE AND THE M3D-K CODE

A. Identification of the TAE

To analyze the MEGA simulation results, we use magnetic flux coordinates (ψ,θ,ϕ), where ψ is the magnetic surface label (in this article, ψ is chosen as $\psi=\sqrt{\bar{\psi}_p}$, where $\bar{\psi}_p$ is the normalized poloidal magnetic flux), ϕ is the usual toroidal angle, and θ is chosen to make magnetic field lines straight on the (θ,ϕ) plane. The perturbations are expanded in terms of the basis function $\exp[i(n\phi+m\theta-\omega t)]$. The results show that the dominant toroidal harmonic is $n=-1$. The mode propagates toroidally in the co-current direction, which is consistent with the general rules for the propagation direction of the ion-driven AEs in tokamaks.[52] Figures 2(a) and 2(b) plot the radial profiles of the sine and cosine parts of various poloidal harmonics of the $n=-1$ component of the perturbed poloidal magnetic field B_θ, which shows that the harmonics with $m=1$ and $m=2$ are dominant and the radial location of the dominant magnetic field perturbation is localized within $\psi=0.4$. Figure 2(c) plots the time evolution of the frequency of the $m/n=1/-1$ component of B_θ in the linear stage, which shows that the mode frequency is about 96 kHz. Figure 2(d) plots the $n=-1$ Alfvén continua calculated by a MHD eigenvalue code,[53] which shows that the mode is within the TAE gap formed due to the coupling of the $m=1$, 2 harmonics. Based on these observations, the mode destabilized in the simulation is identified as a TAE.

B. Comparison of two-dimensional mode structures in the M3D-K code and the MEGA code

Figures 3(a) and 3(b) plot the two-dimensional mode structures in the poloidal plane calculated by the M3D-K code and the MEGA code, respectively. Agreement is found between these two codes as to the dominant poloidal mode numbers [$m=1$, 2 are the dominant poloidal mode numbers with the $m=1$ component larger than the $m=2$ component,

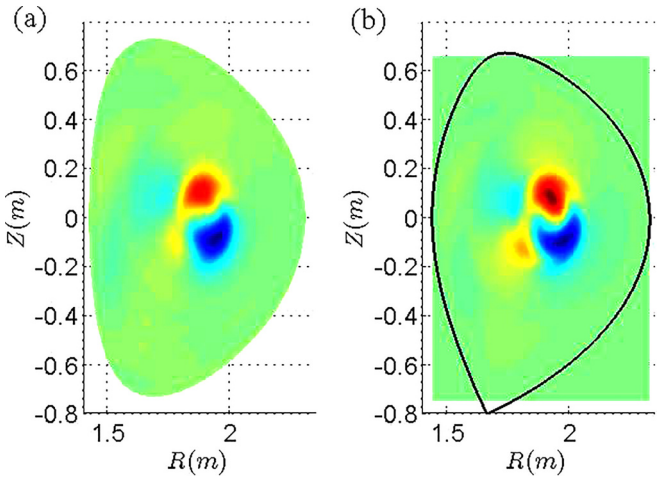

FIG. 3. Contour of the toroidal electric field E_ϕ calculated by the M3D-K code (a) and the MEGA code (b) on the poloidal plane in the linear stage. Also plotted in figure (b) is the LCFS of the equilibrium used by the MEGA code.

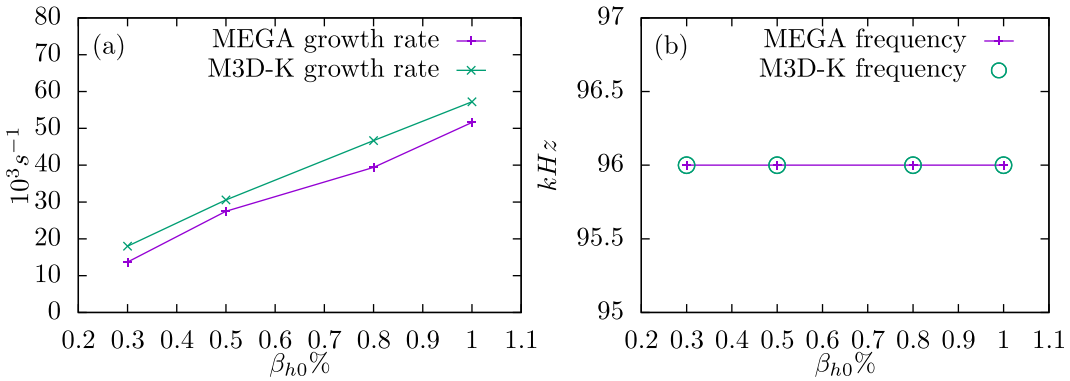

FIG. 4. The TAE growth rate (a) and the real frequency (b) as a function of the fast ion on-axis beta value. The results of MEGA and M3D-K simulations are shown. The other fast ion parameters ($\Lambda_0 = 0.68$, $E_{\text{birth}} = 80\,\text{keV}$) are kept fixed in this parameter scan.

which is consistent with the results shown in Figs. 2(a) and 2(b)] and the spatial location of the mode on the poloidal plane.

C. Comparison of the mode growth rate and the frequency between MEGA and M3D-K codes

Figure 4 plots the mode growth rate and the frequency as a function of the fast ion on-axis beta value β_{h0}. The results indicate that the growth rate and the frequency given by the MEGA code and the M3D-K code agree with each other for different values of β_{h0}. As is shown in Fig. 4(b), the mode frequency given by the two codes is a constant, independent of the EP on-axis beta value. This is consistent with the previous conclusion that the mode is a TAE with the frequency mainly determined by the main plasma.

Figure 5 compares the dependence of the TAE growth rate and the real frequency on the beam injection energy E_{birth} calculated by the two codes. As is shown in Fig. 5(a), the dependence of the mode growth rate on E_{birth} calculated by these two codes shows qualitative agreement, with about 30% relative difference in the high injection energy region. Figure 5(b) shows, as expected, that the mode frequency calculated by both the codes is a constant, independent of E_{birth}.

Figure 6 plots the dependence of the mode growth rate and the real frequency on the central pitch angle parameter Λ_0, which shows that the mode frequency and the growth rate calculated by the two codes agree with each other.

In the parameter scans shown in both Figs. 5(a) and 6(a), there is a peak of the growth rate. The peak in Fig. 5(a) appears at $E_{\text{birth}} = 80\,\text{keV}$ with $\Lambda_0 = 0.68$, while the peak in Fig. 6(a) appears at $\Lambda_0 = 0.65$ with $E_{\text{birth}} = 80\,\text{keV}$. Using the relation $|v_\parallel| = \sqrt{2\varepsilon(1 - \Lambda B/B_0)/m_D}$, where m_D is the mass of the fast ion, we find that both the peaks correspond to $|v_\parallel| \approx V_{A0}/3$.

VI. MEGA SIMULATION RESULTS

A. Resonance interaction between the TAE and fast ions

This section discusses the resonance interaction between the TAE and fast ions simulated by the MEGA code. In the δf particle simulation, a large value of $|\delta f|$ in the phase space usually indicates that the particles in that phase space region are having strong interaction with the wave. Therefore, to identify the particles that are resonant with the TAE, a simple method is to pick out those particles that have a large value of $|\delta f|$. We pick out top 10000 particles with a large value of $|\delta f|$ in the linear stage. To confirm that these particles are indeed resonant with the TAE, we calculate the toroidal and poloidal frequencies, ω_ϕ and ω_θ, of these markers and then examine how well the resonance condition is satisfied. The resonance condition of fast ions with a coherent mode is given by[36]

$$l = \frac{\omega - n\omega_\phi}{\omega_\theta}, \tag{2}$$

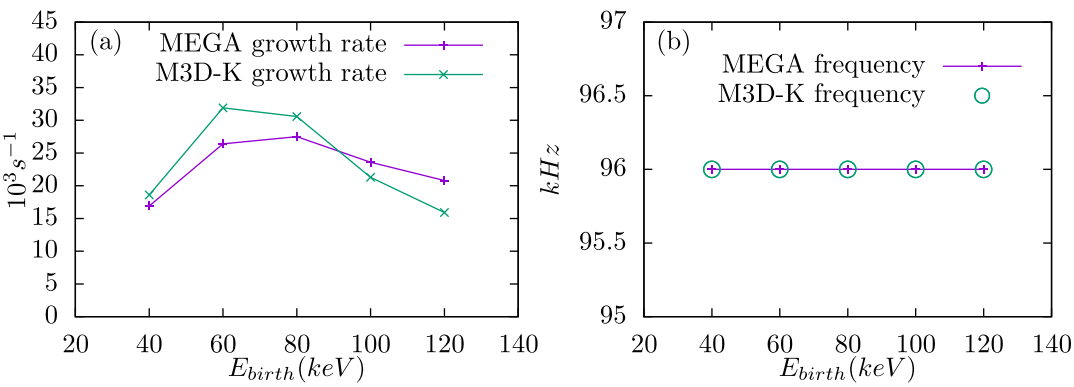

FIG. 5. (a) Comparisons of the TAE growth rate (a) and the frequency (b) calculated by the MEGA code and the M3D-K code for different beam injection energies E_{birth}. The other parameters ($\Lambda_0 = 0.68$, $\beta_{h0} = 0.5\%$) are kept fixed in this parameter scan.

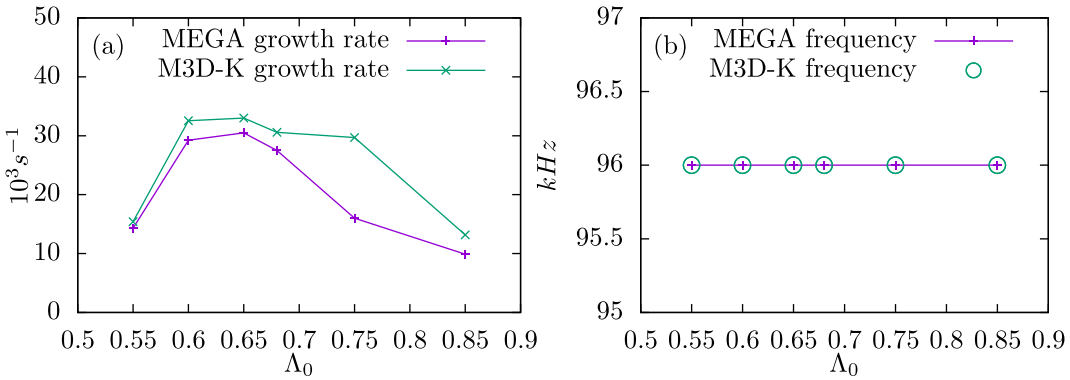

FIG. 6. (a) The TAE growth rate (a) and the frequency (b) as a function of the central pitch angle parameter Λ_0 calculated by the MEGA code and the M3D-K code. The other fast ion parameters ($\beta_{h0} = 0.5\%$, $E_{\text{birth}} = 80\,\text{keV}$) are kept fixed in this parameter scan.

where ω is the frequency of the coherent mode, n is the toroidal mode number, and l is called the resonance number in this paper and should be close to an integer if the particle is resonant with the mode. The values of the resonance number l for the top 10 000 particles chosen above are plotted in Fig. 7(a), which shows that l is close to zero for most of the particles chosen above. This confirms that the resonance condition is well satisfied by these particles, i.e., they are indeed resonant with the TAE.

We found 99% of the top 10 000 particles are strongly passing particles. In this case, the resonance condition (2) can be further simplified. For a strongly circulating particle (i.e., the change in $v_\parallel$ during one poloidal period is small), neglecting the guiding-center orbit width, the poloidal period is approximated by $T_\theta = 2\pi Rq/v_\parallel$, where R is the major radius and q is the safety factor. Thus, the poloidal frequency ω_θ is written as $\omega_\theta = 2\pi/T_\theta = v_\parallel/(qR)$. Similarly, the toroidal angular frequency is written as $\omega_\phi = v_\parallel/R$. Using these, the resonance condition (2) is written as

$$v_\parallel\left(n + \frac{l}{q}\right) = \omega R. \tag{3}$$

On the other hand, the frequency and the radial location of the TAE are approximately given by

$$\omega = \frac{V_{A0}}{2qR}, \tag{4}$$

and

$$q = \left|\frac{2m+1}{2n}\right|, \tag{5}$$

respectively. Substituting Eqs. (4) and (5) into Eq. (3) and using $n = -1$, we obtain

$$v_\parallel = \frac{V_{A0}}{2l - 2m - 1}. \tag{6}$$

For the present case with the resonance number $l = 0$ and dominant poloidal mode numbers $m = 1$, 2, Eq. (6) gives $v_\parallel = -V_{A0}/3$ and $v_\parallel = -V_{A0}/5$. This means that the particles with $v_\parallel = -V_{A0}/3$ or $v_\parallel = -V_{A0}/5$ are resonant with the TAE. This conclusion can be verified by examining the phase-space structure of δf. Figure 7(b) plots the contour (color-map) of the averaged $|\delta f|$ on the $(v_\parallel, \mu)$ plane, which shows that the region with $v_\parallel \approx -V_{A0}/3$ or $v_\parallel \approx -V_{A0}/5$ has a larger value of δf, indicating that these particles are resonant with the TAE. Figure 7(b) also shows that the resonant particles with $v_\parallel \approx -V_{A0}/3$ are dominant compared with those with $v_\parallel \approx -V_{A0}/5$. This is consistent with the fact that the amplitude of the $m = 1$ harmonic is larger than that of the $m = 2$ harmonic.

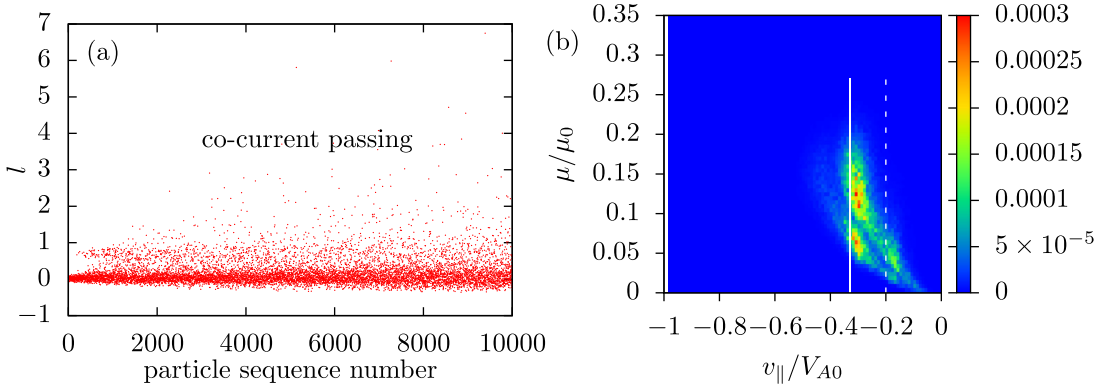

FIG. 7. (a) The values of the resonance number l of the top 10 000 markers with a large value of $|\delta f|$. The markers are sequenced by their magnitude $|\delta f|$ (No. 1 marker has the largest value of $|\delta f|$). The markers with a large sequence number may not be resonant with the TAE, and therefore the resonance number deviates from integers. (b) Contour of averaged $|\delta f|$ on the $(v_\parallel, \mu)$ plane in the linear stage of the mode evolution, where the solid white line indicates the region with $v_\parallel = -V_{A0}/3$ and the white dashed line indicates $v_\parallel = -V_{A0}/5$. Here, $\mu_0 = m_D v_{A0}^2/(2B_0)$.

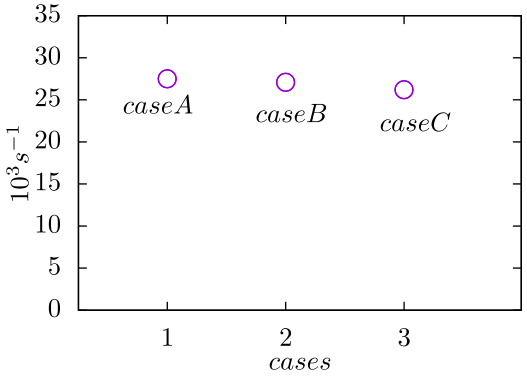

FIG. 8. The TAE growth rate in three cases with different fast ion parameters calculated by the MEGA code. Case A: $\Lambda_0 = 0.68$, $E_{\text{birth}} = 80\,\text{keV}$; case B: $\Lambda_0 = 0.56$, $E_{\text{birth}} = 56\,\text{keV}$; and case C: $\Lambda_0 = 0.37$, $E_{\text{birth}} = 41\,\text{keV}$. The parallel velocity $v_\parallel$ is approximately the same in the three cases.

The above resonant condition can partially explain the dependence of the TAE growth rate on the fast ion parameters shown in Figs. 5(a) and 6(a). Both Figs. 5(a) and 6(a) show that the TAE growth rates reach a peak value near $|v_\parallel| \approx V_{A0}/3$, which is consistent with the conclusion that the TAE is mainly resonant with the particles with $|v_\parallel| \approx V_{A0}/3$. The parallel velocity of most passing fast ions in distribution (1) is given by $v_\parallel \propto \sqrt{\varepsilon} \cdot \sqrt{1-\Lambda}$. With ε or Λ changing away from the value that corresponds to $|v_\parallel| \approx V_{A0}/3$, the fraction of the resonant particles is reduced. Then, the TAE growth rate decreases correspondingly. To further verify this, three simulations with different values of Λ_0 and E_{birth} but with the same value of $v_\parallel$ are carried out. The results are shown in Fig. 8, which indicates that the TAE growth rate remains nearly unchanged in the three cases.

B. Destabilization of the TAE by counter-current passing fast ions

In the above, the TAE is excited by co-current passing fast ions. We also investigate the case with counter-current passing fast ions. We found the same TAE as above is also excited but the growth rate is much smaller compared with the case with co-current passing fast ions. The TAE growth rates of the two cases are compared in Fig. 9(b) at different values of fast ion beta, which shows that the growth rate of the TAE excited by counter-current fast ions is always smaller than that excited by the co-current fast ions. Figure 9(a) plots the typical orbits of the co-current passing particle and the counter-current passing particle on the poloidal plane. From Fig. 9(a), we can observe that the overlapping region between the TAE and the co-current passing fast ions is larger than the counter-current passing fast ions. Thus, the interaction between the TAE and the co-current passing fast ions can be stronger than the counter-current passing fast ions. This partially explains why the co-current fast ions driven TAE has a larger growth rate than that of the counter-current fast ions.

Similar resonance condition analysis as above can be performed for the counter-current passing fast ions. Figure 10(a) plots the values of the resonance number l calculated by Eq. (2) for counter-current passing fast ions, which shows that $l \approx 3$ for most of the particles with a large value of $|\delta f|$. The contour of the averaged $|\delta f|$ on the $(v_\parallel, \mu)$ plane is plotted in Fig. 10(b), which shows that the fast ions with parallel velocity $v_\parallel \approx V_{A0}/3$ exchange energy with the TAE. This parallel velocity is consistent with the results calculated by Eq. (6) with $m = 1$ and $l \approx 3$. The interaction between the particles and the TAE is weak for $l = 3$ and the $m = 1$ harmonic when the interaction is integrated in the poloidal angle. Stronger interaction can be expected for $l = 3$ and the $m = 2$ poloidal harmonic, but the $m = 2$ harmonic of the TAE is weak. Then, the smaller growth rates for the counter-current passing particles can be partially attributed to the resonance with $l = 3$.

VII. SUMMARY

This article presents a linear benchmark between two kinetic-MHD hybrid codes, MEGA and M3D-K, for the fast

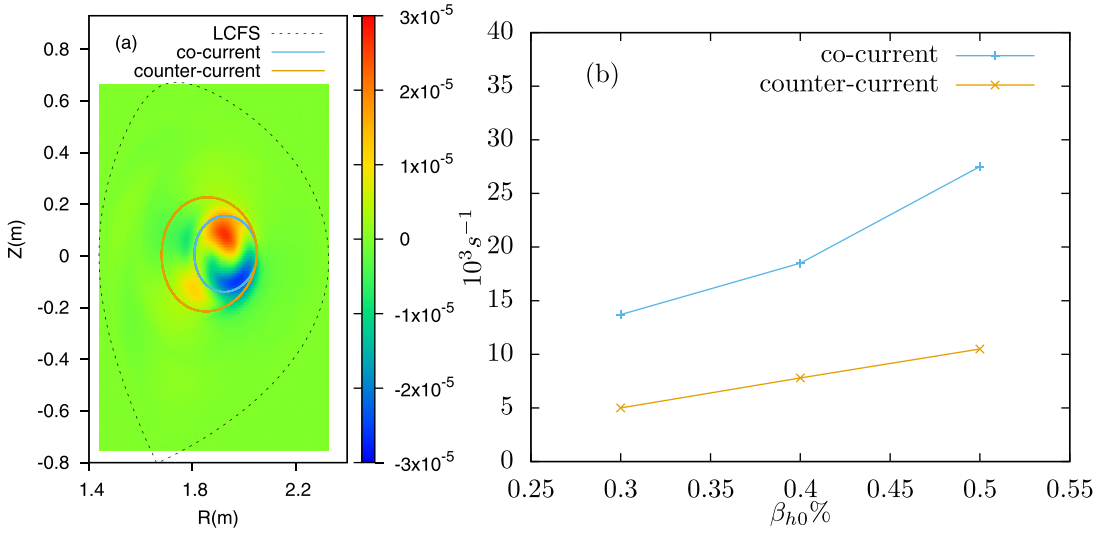

FIG. 9. (a) The mode structure of the TAE calculated by the MEGA code. Also plotted on (a) are typical orbits of co-current and counter-current passing particles with $E_{\text{birth}} = 80\,\text{keV}$, $\Lambda = 0.68$ and the birth location at $(R = 2.1\,\text{m}, Z = 0\,\text{m})$ on the poloidal plane. (b) The dependence of the growth rate of the TAE destabilized by co-current and counter-current passing particles on the fast ion on-axis beta value β_{h0}. The other parameters of the fast ion distribution are fixed ($E_{\text{birth}} = 80\,\text{keV}$, $\Lambda_0 = 0.68$).

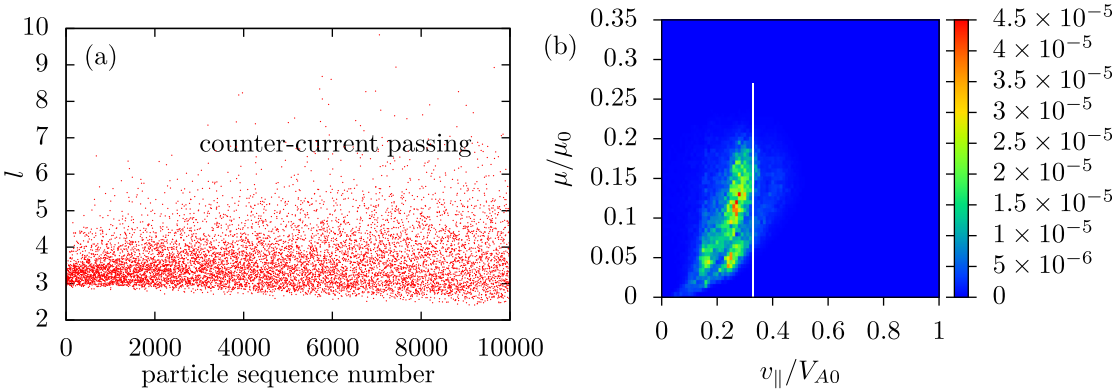

FIG. 10. (a) The values of the resonance number l of the top 10 000 markers with a large value of $|\delta f|$. (b) Contour of averaged $|\delta f|$ on the $(v_\parallel, \mu)$ plane in the linear stage of the mode evolution, where the white line indicates the location $v_\parallel = V_{A0}/3$.

ion driven toroidal Alfvén eigenmodes in a realistic EAST plasma. The results show good agreement between the two codes with respect to the dependence of the TAE growth rate and the real frequency on the fast ion on-axis beta β_{h0}, the injection beam energy E_{birth} and the central pitch angle parameter Λ_0. To better understand the details of the interaction between the TAE and fast ions, a series of simulations are carried out by using the MEGA code. The results show that the TAE is resonant with the co-current passing particles with the parallel velocity $v_\parallel \approx -V_{A0}/3$ or $v_\parallel \approx -V_{A0}/5$. In addition, the TAE destabilized by the counter-current passing ions is also analyzed and found to have much smaller growth rate than that of the co-current fast ion driven TAE. One of the reasons for this is found to be that the counter-current passing fast ion orbits lie on the radial edge of the TAE, and thus the wave-particle energy exchange is not efficient.

ACKNOWLEDGMENTS

The authors acknowledge useful discussions with G. Y. Fu, G. Q. Li, J. Zhu, and W. J. Wang. Numerical computations were performed on the ShenMa High Performance Computing Cluster at the Institute of Plasma Physics, Chinese Academy of Sciences. This work was partially supported by National Key R&D Program of China under Grant No. 2017YFE0300400, National Natural Science Foundation of China under Grant Nos. 11475220, 11575251, 11575249, and 11605245, and National Magnetic Confinement Fusion Energy Research Program under Grant No. 2015GB110005.

[1]G. Y. Fu and J. W. V. Dam, Phys. Fluids B **1**, 1949 (1989).
[2]L. Chen, Phys. Plasmas **1**, 1519 (1994).
[3]B. N. Breizman and S. E. Sharapov, Plasma Phys. Controlled Fusion **53**, 054001 (2011).
[4]C. Cheng, L. Chen, and M. Chance, Ann. Phys. **161**, 21 (1985).
[5]R. Nazikian, G. Y. Fu, Z. Chang, S. H. Batha, H. Berk, R. V. Budny, Y. Chen, C. Z. Cheng, D. S. Darrow, N. N. Gorelenkov, F. M. Levinton, S. Medley, M. P. Petrov, M. Redi, E. Ruskov, D. A. Spong, R. B. White, and S. J. Zweben, Phys. Plasmas **5**, 1703 (1998).
[6]K. L. Wong, Plasma Phys. Controlled Fusion **41**, R1 (1999).
[7]W. W. Heidbrink, Phys. Plasmas **15**, 055501 (2008).
[8]N. Gorelenkov, S. Bernabei, C. Cheng, K. Hill, R. Nazikian, S. Kaye, Y. Kusama, G. Kramer, K. Shinohara, T. Ozeki, and M. Gorelenkova, Nucl. Fusion **40**, 1311 (2000).
[9]W. Heidbrink and G. Sadler, Nucl. Fusion **34**, 535 (1994).
[10]M. A. V. Zeeland, W. W. Heidbrink, R. K. Fisher, M. G. Muñoz, G. J. Kramer, D. C. Pace, R. B. White, S. Aekaeslompolo, M. E. Austin, J. E. Boom, I. G. J. Classen, S. da Graça, B. Geiger, M. Gorelenkova, N. N. Gorelenkov, A. W. Hyatt, N. Luhmann, M. Maraschek, G. R. McKee, R. A. Moyer, C. M. Muscatello, R. Nazikian, H. Park, S. Sharapov, W. Suttrop, G. Tardini, B. J. Tobias, Y. B. Zhu, DIII-D, and A. U. Teams, Phys. Plasmas **18**, 056114 (2011).
[11]R. B. White, E. Fredrickson, D. Darrow, M. Zarnstorff, R. Wilson, S. Zweben, K. Hill, Y. Chen, and G. Fu, Phys. Plasmas **2**, 2871 (1995).
[12]W. W. Heidbrink, N. N. Gorelenkov, Y. Luo, M. A. Van Zeeland, R. B. White, M. E. Austin, K. H. Burrell, G. J. Kramer, M. A. Makowski, G. R. McKee, and R. Nazikian, Phys. Rev. Lett. **99**, 245002 (2007).
[13]Y. Todo, H. L. Berk, and B. N. Breizman, Phys. Plasmas **10**, 2888 (2003).
[14]R. B. White, N. Gorelenkov, W. W. Heidbrink, and M. A. V. Zeeland, Phys. Plasmas **17**, 056107 (2010).
[15]D. J. Sigmar, C. T. Hsu, R. White, and C. Z. Cheng, Phys. Fluids B **4**, 1506 (1992).
[16]S. D. Pinches, I. T. Chapman, P. W. Lauber, H. J. C. Oliver, S. E. Sharapov, K. Shinohara, and K. Tani, Phys. Plasmas **22**, 021807 (2015).
[17]K. L. Wong, R. J. Fonck, S. F. Paul, D. R. Roberts, E. D. Fredrickson, R. Nazikian, H. K. Park, M. Bell, N. L. Bretz, R. Budny, S. Cohen, G. W. Hammett, F. C. Jobes, D. M. Meade, S. S. Medley, D. Mueller, Y. Nagayama, D. K. Owens, and E. J. Synakowski, Phys. Rev. Lett. **66**, 1874 (1991).
[18]W. Heidbrink, E. Strait, E. Doyle, G. Sager, and R. Snider, Nucl. Fusion **31**, 1635 (1991).
[19]ITER Physics Basis Editors, Nucl. Fusion **39**, 2471 (1999).
[20]W. Chen, M. Jiang, Y. Xu, P. Shi, L. Yu, X. Ding, Z. Shi, X. Ji, D. Yu, Y. Li, Z. Yang, W. Zhong, Z. Qiu, J. Li, J. Dong, Q. Yang, Y. Liu, L. Yan, M. Xu, and X. Duan, Nucl. Fusion **57**, 114003 (2017).
[21]G. Vlad, S. Briguglio, G. Fogaccia, F. Zonca, C. D. Troia, W. Heidbrink, M. V. Zeeland, A. Bierwage, and X. Wang, Nucl. Fusion **49**, 075024 (2009).
[22]J. Zhu, Z. Ma, and G. Fu, Nucl. Fusion **54**, 123020 (2014).
[23]F. Zonca and L. Chen, Phys. Plasmas **21**, 072120 (2014).
[24]W. Zhang, I. Holod, Z. Lin, and Y. Xiao, Phys. Plasmas **19**, 022507 (2012).
[25]X. Wang, S. Briguglio, L. Chen, C. D. Troia, G. Fogaccia, G. Vlad, and F. Zonca, Phys. Plasmas **18**, 052504 (2011).
[26]G. Fogaccia, G. Vlad, and S. Briguglio, Nucl. Fusion **56**, 112004 (2016).
[27]D. A. Spong, B. A. Carreras, and C. L. Hedrick, Phys. Fluids B **4**, 3316 (1992).
[28]S. Briguglio, G. Vlad, F. Zonca, and C. Kar, Phys. Plasmas **2**, 3711 (1995).
[29]Y. Todo, T. Sato, K. Watanabe, T. H. Watanabe, and R. Horiuchi, Phys. Plasmas **2**, 2711 (1995).
[30]W. Park, S. Parker, H. Biglari, M. Chance, L. Chen, C. Z. Cheng, T. S. Hahm, W. W. Lee, R. Kulsrud, D. Monticello, L. Sugiyama, and R. White, Phys. Fluids B **4**, 2033 (1992).
[31]D. Borba, H. Berk, B. Breizman, A. Fasoli, F. Nabais, S. Pinches, S. Sharapov, and D. Testa, and Contributors to the EFDA-JET Workprogramme, Nucl. Fusion **42**, 1029 (2002).

[32]A. Mishchenko, A. Könies, and R. Hatzky, Phys. Plasmas **16**, 082105 (2009).
[33]W. Deng, Z. Lin, I. Holod, X. Wang, Y. Xiao, and W. Zhang, Phys. Plasmas **17**, 112504 (2010).
[34]M. D. J. Cole, A. Mishchenko, A. Könies, R. Hatzky, and R. Kleiber, Plasma Phys. Controlled Fusion **57**, 054013 (2015).
[35]Y. Chen and S. E. Parker, Phys. Plasmas **18**, 055703 (2011).
[36]Y. Todo and T. Sato, Phys. Plasmas **5**, 1321 (1998).
[37]Y. Todo, K. Shinohara, M. Takechi, and M. Ishikawa, Phys. Plasmas **12**, 012503 (2005).
[38]Y. Todo, Phys. Plasmas **13**, 082503 (2006).
[39]W. Park, E. V. Belova, G. Y. Fu, X. Z. Tang, H. R. Strauss, and L. E. Sugiyama, Phys. Plasmas **6**, 1796 (1999).
[40]Y. Todo, H. Berk, and B. Breizman, Nucl. Fusion **50**, 084016 (2010).
[41]Y. Pei, N. Xiang, Y. Hu, Y. Todo, G. Li, W. Shen, and L. Xu, Phys. Plasmas **24**, 032507 (2017).
[42]G. Y. Fu, W. Park, H. R. Strauss, J. Breslau, J. Chen, S. Jardin, and L. E. Sugiyama, Phys. Plasmas **13**, 052517 (2006).
[43]W. Shen, G. Y. Fu, B. Tobias, M. V. Zeeland, F. Wang, and Z. M. Sheng, Phys. Plasmas **22**, 042510 (2015).
[44]F. Wang, G. Y. Fu, J. A. Breslau, and J. Y. Liu, Phys. Plasmas **20**, 102506 (2013).
[45]D. Liu, G. Y. Fu, N. A. Crocker, M. Podestá, J. A. Breslau, E. D. Fredrickson, and S. Kubota, Phys. Plasmas **22**, 042509 (2015).
[46]G. Q. Li, Q. L. Ren, J. P. Qian, L. L. Lao, S. Y. Ding, Y. J. Chen, Z. X. Liu, B. Lu, and Q. Zang, Plasma Phys. Controlled Fusion **55**, 125008 (2013).
[47]R. G. Littlejohn, J. Plasma Phys. **29**, 111 (1983).
[48]A. Dimits and W. Lee, J. Comput. Phys. **107**, 309 (1993).
[49]S. E. Parker and W. W. Lee, Phys. Fluids B **5**, 77 (1993).
[50]L. Lao, H. S. John, R. Stambaugh, and W. Pfeiffer, Nucl. Fusion **25**, 1421 (1985).
[51]S. Hirshman, W. van RIJ, and P. Merkel, Comput. Phys. Commun. **43**, 143 (1986).
[52]Y. Todo, AIP Conf. Proc. **1478**, 141 (2012).
[53]Y. Hu, G. Li, N. N. Gorelenkov, H. Cai, W. Yang, D. Zhou, and Q. Ren, Phys. Plasmas **21**, 052510 (2014).